Design and Analysis of Enhanced Modulation Response in Integrated Coupled Cavities DBR Lasers Using Photon-Photon Resonance

Paolo Bardella, Weng W. Chow and Ivo Montrosset, Member, IEEE

Abstract—In the last decades, various solutions have been proposed to increase the modulation bandwidth and consequently the transmission bit rate of integrated semiconductor lasers. In this manuscript we discuss a design procedure for a recently proposed laser structure realized with the integration of two DBR lasers. Design guidelines will be proposed and dynamic small and large signal simulations, calculated using a Finite Difference Traveling Wave numerical simulator, will be performed to confirm the design results and the effectiveness of the analyzed integrated configuration to achieve a direct modulation bandwidth up to $80\,\mathrm{GHz}$.

Index Terms—Semiconductor laser diode; monolithically integrated coupled-cavity DBR lasers; integrated optics; photonic integrated circuits (PICs); direct modulation; small-signal modulation bandwidth; eye diagram; DBR laser; optical injection locking.

I. Introduction

S EMiconductor laser diodes with wide direct modulation bandwidth represent an important element to fulfill the continuously increasing request for low-cost optical communications systems with high bit-rate (see, e.g., [1]). Whilst the maximum bit-rate achieved by direct modulated lasers is typically limited by the well-known resonance between carriers and photons (Carrier-Photon Resonance, CPR) [2], many solutions have been proposed to overcome this restriction, see for example [3] for a review.

A first mechanism identified to extend the modulation bandwidth is the detuned loading (DL) due to the dispersion effect introduced by a coupled passive cavity [4], [5] or by a distributed mirror (DBR [6]–[8] or DFB [9]) when the lasing mode is properly positioned at a slightly higher wavelength respect to the minimum threshold gain condition.

A second approach used to extend the lasers dynamic properties is to take advantage, in a properly designed cavity, of the interaction between the lasing mode and an adjacent longitudinal cavity mode so that they can interact thanks to the carrier pulsation introduced by the current modulation applied at the gain section electrode [6], [7], [10]–[12]. This interaction introduces a resonance in the intensity modulation response at the frequency corresponding to the two cavity modes separation; such a resonance is frequently called Photon-Photon Resonance (PPR).

Since the PPR usually occurs at a frequency which is much higher than the CPR frequency, the request for an almost flat

P. Bardella and I. Montrosset are with the Dipartimento di Elettronica e Telecomunicazioni, Politecnico di Torino, Corso Duca degli Abruzzi 24, 10129 Torino, Italy W. W. Chow is with Sandia National Laboratories, Albuquerque, NM 87185 USA email: paolo.bardella@polito.it

Manuscript received xxx, 2015; revised YYY, 2015.

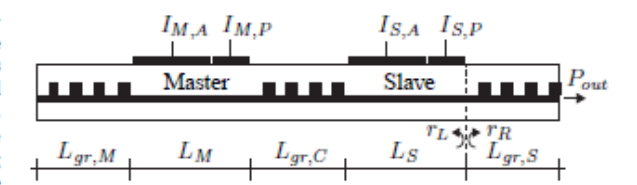


Fig. 1: Schematics of the considered coupled cavities DBR laser. L_M and L_S are the sum of the lengths of the active and phase-control sections of the two laser cavities. The currents $I_{M,A}$ ($I_{M,P}$) and $I_{S,A}$ ($I_{S,P}$) are injected in the active (phase-control) sections of the Master (left) and Slave (right) laser cavities, respectively. The dashed line indicates the reference plane at which the left (r_L) and right (r_R) equivalent reflectivities are calculated using the transfer matrix method.

modulation response implies the need of a proper cavity design to have the PPR at the correct frequency. If this condition is not satisfied, the gap between the PPR and CPR peaks could make the device useless for many telecommunication applications.

An approach which is frequently used to achieve this condition is the introduction of an external feedback to the laser cavity. On this concept, various cavity designs have been studied and realized as, e.g., the Complex Cavity Injection Grating (CCIG) [13]-[16], DFB with integrated Feedback (IFB-DFB) [17], or single mode cavity with feedback effects [18], [19]. Furthermore the modulation bandwidth extension. can be obtained using the injection-locking [20]-[22] to the optical signal of an external source. The modulation bandwidth extension has also been obtained exploiting the coupling between two modes in a waveguide supporting two transverse modes [23] or coupled cavity VCSELs [24], [25]. In all the previously cited cases, the bandwidth extension by PPR can be used either a) to improve the dynamic characteristics of a laser which shows a limited modulation bandwidth because of its non-optimal material [26] or cavity [1] properties, or b) to extend the dynamic properties of a device which already exhibits a good modulation response.

The structure investigated in this manuscript consists in two coupled cavity DBR lasers integrated in a single chip as schematically reported in Fig. 1. This structure can be seen both as an example of a DBR laser with an external feedback from an active cavity or as an integrated injection-locked DBR laser as it has been already presented in [27]–[30] depending on the injection level in the two cavities. In all cases considered in this paper, just for simplicity, we will call Master the unmodulated cavity and Slave the other one.

The additional contributions in this paper respect to the previous ones are: the definition of a design procedure allow-

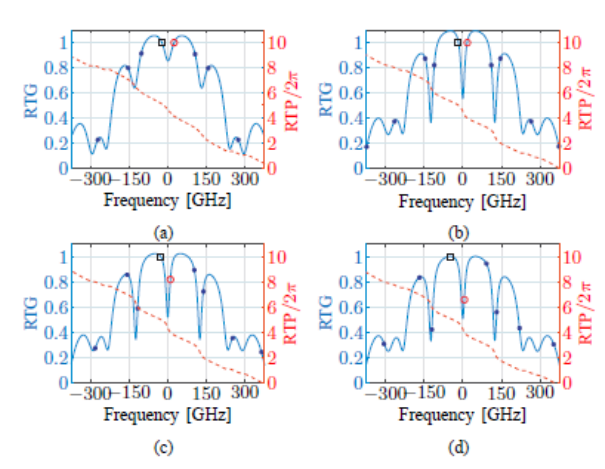


Fig. 2: RTG (continuous blue line) and RTP (dashed red line) functions plots at threshold around the Bragg frequency. The lasing mode is indicated by the black square, the closest non lasing mode by the red circular marker and the other non-lasing modes by the blue markers. $L_{gr,M}=180~\mu m$, $L_M=L_S=250~\mu m$, $L_{gr,S}=70~\mu m$, $\kappa=100~c m^{-1}$. In (a) the central grating length is $L_{gr,C}=42~\mu m$ and the fppp is 50 GHz. In (b) $L_{gr,C}=82~\mu m$ and $fppp_R=35~GHz$. In (c) and (d) the position of the modes is changed respect to (b) becuase of the introduction of an additional phase shift ϕ_S in the Slave laser section: in (c) $\phi=\pi/4$ and $fpp_R=40~GHz$; in (d) $\phi=\pi/2$ and $fpp_R=60~GHz$. The cavity parameters used in (b-d) correspond to the square marker indicated in Fig. 4b.

ing to determine the cavity parameters necessary to achieve a prescribed PPR frequency ($f_{\rm PPR}$) and the validation of the design results by showing the possibility of large signal operation conditions with clearly open eye diagram at an higher bit rate respect to that of the single cavity configuration.

The paper is organized as follow: first in Section II we will present the novel proposed cavity design procedure and the obtained cavity design maps; in Section III the results from small and large signal modulation for the designed structure will be discussed. Finally in Section IV we will draw the Conclusions.

II. DESIGN OF THE COUPLED DBR LASERS CAVITY

For the composite DBR cavity under consideration (Fig. 1) as well as for the other cases referenced in Section I, a proper choice of the cavity parameters is the essence for the exploitation of the mode coupling mechanism between the lasing mode and the nearest one. The need of a design derives from the fact that, if the cavity wants to be kept short to avoid parasitic effect limiting the laser dynamic, the mode separation is usually too high to obtain a flat dynamic modulation response. Therefore, a proper design of the cavity is needed in order to control the separation between the two modes that should interact to obtain the modulation extension effect. The precise mode separation can only be obtained from the above-threshold analysis [16], [17], but an analysis at threshold [12], [13] allows a very good estimate of it. Thus, the results found at threshold will be used to define the structure to be analyzed in the above-threshold simulations. Being interested in the case in which both cavities are above threshold with independent current injection in the active

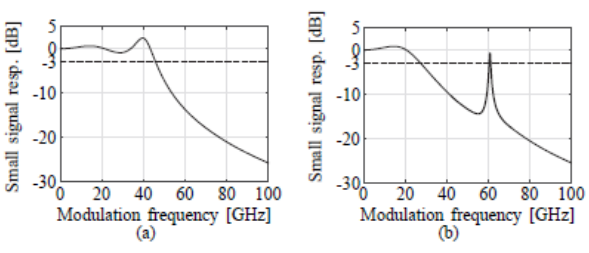


Fig. 3: Examples of small signal modulation responses obtained for the cases in Fig. 2c,d

regions, only for the below threshold analysis, we assumed the active section of the Master (left) cavity at transparency and we searched the threshold condition of the full coupled cavities structure assuming gain only in the Slave (right) cavity. Furthermore to emphasize the role of the cavities in the lasing mode selection we assumed for this threshold analysis a wavelength independent gain function. In this condition we computed at threshold the gain and frequency of the lasing mode and of the adjacent ones and the round trip gain (RTG) and phase (RTP) function of the full cavity in the frequency range around the lasing mode. The RTG and RTP functions at the lasing condition have been computed making reference at the input section of the right grating of the Slave laser section (dashed vertical line in Fig. 1); the left (r_L) and right (r_R) equivalent reflectivities have been computed using the transmission matrix approach [2] from which follows

$$RTG = |r_L r_R|$$
; $RTP = \angle r_L r_R$.

This analysis allows to obtain the frequency separation between the lasing and the adjacent modes. It also gives a preliminary information on the mode competition from the gain margin between the lasing mode and the non lasing ones. Two examples of the results for the RTG and RTP functions around the lasing frequency are reported in Fig. 2 for two cases obtained by changing the central DBR grating maximum reflectivity R_C . The FSR of the composite cavity in the case of a very weak central reflectivity is 75 GHz while in the cases reported in Fig. 2 the separation $f_{\rm PPR}$ between the lasing mode (black marker) and the adjacent one (red marker) is reduced to 50 GHz for $R_C=15\,\%$ (Fig. 2a) and to 35 GHz for $R_C=42\,\%$ (Fig. 2b). The highlighted behavior clearly shows the role of the central grating reflectivity and the need of weakly coupled cavities to reduce $f_{\rm PPR}$ to a suitable value.

Furthermore the above reported conditions are not automatically obtained since a small change in the effective optical length in any of the two cavities introduces a mode shift which can alter the composite cavity modes separation. An example is reported in Fig. 2c d, where we present the results obtained introducing a $\pi/4$ (Fig. 2c) and $\pi/2$ (Fig. 2d) phase shift in the Slave cavity respect to the case considered in Fig. 2b.

The difference, respect to Fig.2b, in the separation between the lasing mode and the adjacent one allows in the first case to obtain a small signal response useful for practical application in digital transmission experiments while in the other case the PPR frequency is too high. An example of the small signal modulation characteristics in these cases is shown in Fig. 3. It

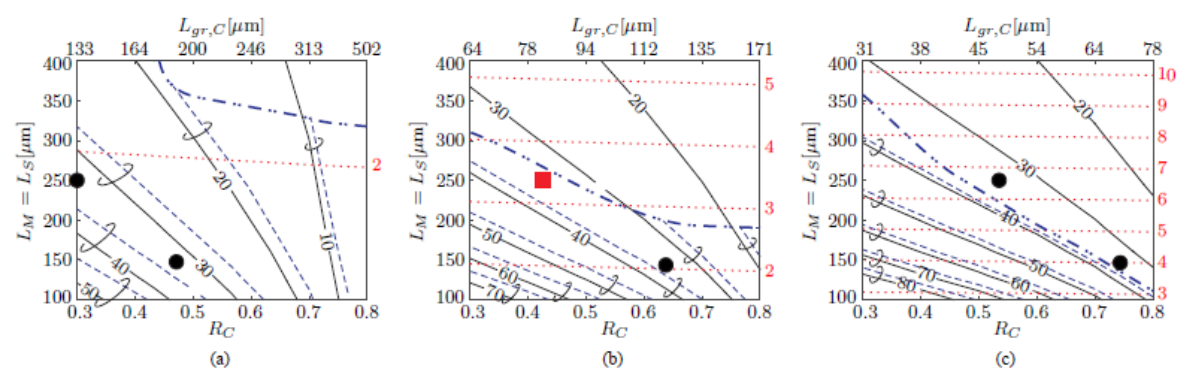


Fig. 4: Coupled cavities DBR laser design maps for equal cavities length $(L_M=L_S)$: PPR frequency (in GHz) as function of the central grating reflectivity (R_C) and for cleaved (continuous lines map) and grating (dashed lines map) right facet with the same maximum reflectivity $R_R=32\,\%$. Results are obtained for a lossless left reflectivity $R_L=90\,\%$ and with $\kappa=50\,\mathrm{cm}^{-1}$ (a), $\kappa=100\,\mathrm{cm}^{-1}$ (b), and $\kappa=200\,\mathrm{cm}^{-1}$ (c). In the area where the constant frequency lines are not reported the PPR conditions are more critical to be found due to mode competition. The red dashed lines indicate the number of the full cavity modes inside the main lobe of the reflectivity curve. The large round markers indicate the structures which we have analyzed in their small and large signal modulation responses while the square marker indicates the structure whose dynamic results have been reported in this paper.

is therefore important to define a design procedure allowing to give an estimate of the PPR frequency in the modulation response as a function of the complete-cavity parameters and then to have also the possibility to tune the modes position in such a way that the laser can operate in optimized conditions.

Differently from previous studies [27], [28], in our analysis the distributed characteristics of the DBR mirrors have been considered and therefore the cavities parameters for the laser design are:

- the three DBR mirrors maximum reflectivities (R_L, R_C, R_R) or the corresponding lengths (L_{gr,M}, L_{gr,C}, L_{gr,S}) when assuming the coupling coefficient κ to be the same for all the gratings;
- the length of the right cavity L_S and the cavity length ratio AMS = L_M/L_S.

The design analysis has been done first by choosing the parameters of the two DBR cavities imposing the condition that both the cavities in isolation must be lasing at the mirrors common Bragg frequency. This condition will imply for the composite cavity the presence of two closely spaced full cavity resonances, separated by a quantity proportional to the cavities coupling strength. In proper operation conditions above threshold, the coupling between these two cavity modes due to the current modulation can produce the extra PPR in the small signal modulation response [12], [16] allowing the possibility to extend the laser modulation bandwidth.

A first step in the cavity design is the definition of the role of the two lasers. Since we assumed that the Slave (right DBR) laser will be modulated, the output power will be from the right mirror. The second assumption is that the Master (left DBR) laser has only a small output power on the left side of the cavity in order to maximize its power coupling to the Slave laser. Obviously, with these assumptions the maximum reflectivity will be that of the left DBR mirror (R_L) and the minimum reflectivity that of the right one (R_R) . The value of the central mirror reflectivity (R_C) will be in between R_L and R_R and will determine the strength of the coupling between the two cavities and consequently the frequency splitting $f_{\rm PPR}$

between the resonances of the composite cavity.

In order to have a first estimate of the achievable range of the full cavity $f_{\rm PPR}$, this frequency was computed choosing the value of the lossless left grating reflectivity R_L and assuming the output right facet to be either cleaved, for realization simplicity, or realized with a grating with maximum reflectivity $R_R=32\,\%$. Three values of the grating coupling coefficient ($\kappa=50,100,\,200\,{\rm cm^{-1}}$) were considered and the waveguides and grating losses were assumed to be $10\,{\rm cm^{-1}}$. The remaining cavity parameters (central grating reflectivity R_C and the total Master and Slave cavity lengths L_S and L_M) have been considered to be variable parameters; for this first analysis we assume AMS = 1. Results and considerations for different values of AMS will be reported in the following.

All these results have been represented in Fig. 4 in which we kept constant the left grating reflectivity $R_L=90\,\%$ and we considered as parameters for each figure the coupling coefficient κ . These figures are fundamental to select the structures to consider also on the basis of the available technology for the grating realization and the active material gain characteristics.

In Fig. 4 maps the f_{PPR} is represented both for the case of cleaved and grating output facet with continuous and dashed lines, respectively. A parameter is also reported, representing the number of the cavity modes inside the central reflectivity lobe of the composite cavity reflectivity r_L indicated in Fig. 1. This parameter is important because the larger is its value the greater is the possibility of competition between the lasing mode and the adjacent ones which can lead to instabilities in the output power. As can be seen from the maps in Fig. 4 a broad range of f_{PPR} , from 10 to 80 GHz can be obtained. As we predicted small f_{PPR} values are obtained for higher value of the central grating reflectivity R_C due to the weak coupling between the two cavities, while the opposite is obtained for smaller values. Obviously also the right cavity length L_R affects f_{PPR} that decreases for larger values of L_R because of the reduction of the cavity FSR. The regions in Fig. 4 maps where the constant PPR frequency lines have not been reported indicates operation conditions in which, with the

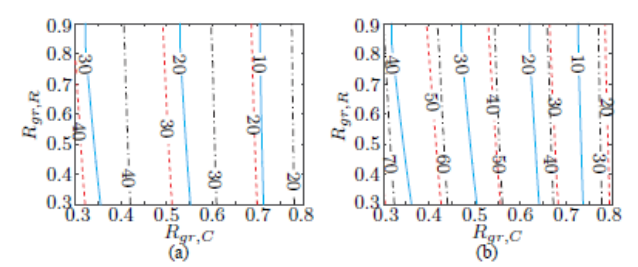


Fig. 5: PPR frequency as function of the maximum central grating reflectivity R_C and the maximum right grating reflectivity R_R , for active sections length $L_M=L_S=150\,\mu\mathrm{m}$ (a) and $L_M=L_S=250\,\mu\mathrm{m}$ (b). Three values of the grating coupling coefficient are considered: $\kappa=50\,\mathrm{cm}^{-1}$ (continuous lines, labels on the top), $\kappa=100\,\mathrm{cm}^{-1}$ (dashed lines, labels in the middle), $\kappa=200\,\mathrm{cm}^{-1}$ (dashed-dotted lines, labels on the bottom). The left grating maximum reflectivity is $90\,\%$.

approximation used to generate the maps, the gain margin respect to the other modes of the cavity is very small or lasing can be found at frequencies shifted from the Bragg condition due to the complexity of the reflectivity curve. The latter behavior is usually due to the higher number of cavity modes inside the main reflectivity lobe of r_L . From our experience, in these regions the extended modulation bandwidth conditions could still be obtained, but they are more critical to be found and the role of the shift between the Bragg condition and the gain peak becomes important to determine the operation conditions. To simplify the reading of the maps, the truncation points have been connected with a thick dash-point blue line. As it can be seen, the frequency selection introduced using a Bragg grating at the output facet instead of a cleaved surface allows to extend the f_{PPR} curves over all the considered parameters range.

The previous analysis has been done also for different lengths of the two sections (AMR \neq 1) while keeping constant the total length; the results show a significant reduction of the PPR frequency and an increase of the area of mode competition as long as the Master cavity length is reduced. We therefore present in the following results only for the case of equal cavity lengths.

To quantitatively present the fundamental role of the central grating reflectivity on the $f_{\rm PPR}$, the map in Fig. 5 shows its value when R_R and R_C are varied for a constant value of $R_L=0.90$ and two values of $L_L=L_R=150\,\mu{\rm m}$ and $250\,\mu{\rm m}$. The estimated values of $f_{\rm PPR}$ show a large independence from R_R and significant dependence on κ due to the change of the effective grating length for a given R_C value.

III. DYNAMIC CHARACTERISTICS

Recently the small signal properties of the two integrated DBR laser structures have been analyzed using composite mode theory [27], [28] and also experimentally realized and characterized [28], [29] respect to their small signal modulation response.

In this section we report the results of the dynamic simulations using our Finite Difference Traveling Wave (FDTW) numerical code [31]. These simulations have as objectives

the verification of operation conditions showing the presence of the PPR in the small signal modulation bandwidth to confirming the results of the previous static design procedure in Section II, but their aim is also to show the existence of extended modulation bandwidth conditions allowing the possibility of digital data transmission at higher bit rate respect to a what obtainable in similar DBR lasers.

As highlighted in Fig. 2, a fine tuning of the longitudinal cavity modes position is generally required to obtained the modulation bandwidth enhancement. In real devices, this tuning is generally accomplished using the phase-control sections currents $I_{M,P}$ and $I_{S,P}$ (Fig. 1). In the following simulations, for consistency with the presented analysis at threshold and in order to simplify the results interpretations, we simply added a fictitious phase contribution ϕ_M to the electric field propagating in the Slave laser section.

We simulated the 6 laser cavities which we indicated with markers in Fig. 6 maps. We have chosen cavities with a PPR around $35\,\mathrm{GHz}$ and between the various options we considered the cases with a short cavity lengths to be sure against limitations due to parasitic effects for high bit rate transmission. Furthermore we have decided to operate with cavity parameters allowing only a limited number of longitudinal modes in the r_L main reflectivity lobe allowing to use for simplicity an output cleaved facet. The material and waveguide parameter used in the simulation are reported in Table I.

The obtained small signal modulation results present a very similar behavior for all the considered structures and for the currents in the active and phase control sections. In the map in Fig. 6a we summarize the obtained behavior in the plane of the active Master and Slave section currents normalized respect to the value at the threshold of each DBR in isolation.

In the upper part of the map, indicated with the label (A-SP), we obtained typically in our structures the presence of two lasing modes with a variable spectral power ratio depending on the normalized currents combination in the two active sections and on the phase control sections currents. In the two example shown in Fig.7 we report two cases of self-pulsation operation found when the two active section currents are the same and for two values of the phase control currents. The phase control allows to shift the oscillation frequency from the minimum value of the PPR frequency obtained in the previously reported design procedure to higher values. The results show in both cases the possibility to obtain a good extinction ratio and a narrow RF spectra.

In the region (B), with higher aster section current, for a wide range of the control phase, single mode operation has been obtained and examples of the corresponding small signal modulation characteristics have been reported in Fig. 6b. Obviously these operation conditions are not adapted for the digital modulation we are looking for.

Also in region (D) of higher Slave injection current the single mode behavior in CW is obtained over a wide range of the control phase and the modulation results shown in Fig. 6d allows to predict the possibility to obtain operations with large signal modulation bandwidth extension. In region (C) operation condition in between those previously described in regions (B) and (D) are obtained as shown in Fig. 6c.

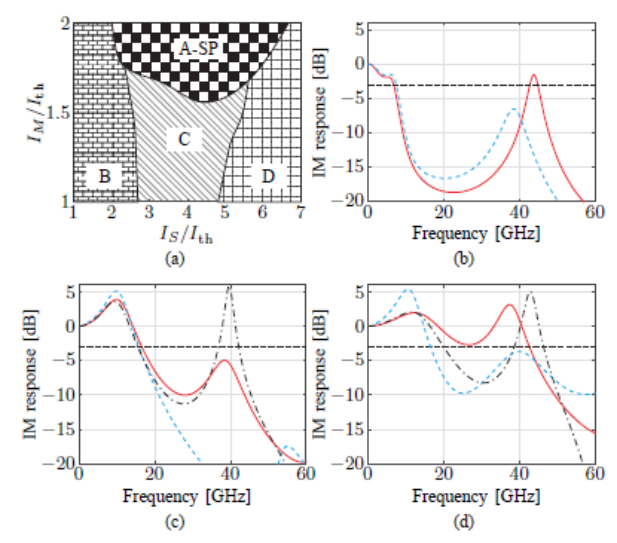


Fig. 6: Small signal dynamic results for the structure characterized by the square point in Fig. 5b. (a) Map in the normalized Master and Slave active sections currents plane indicating the four behaviors which are typically found. In the (A-SP) region periodic self-pulsation (see Fig. 7 can be found. Examples of the typical dynamic response obtained with different values of ϕ_S in B, C, D regions are reported in parts (b), (c), (d) of this figure. The horizontal dashed lines represent the -3 dB level for the modulation response.

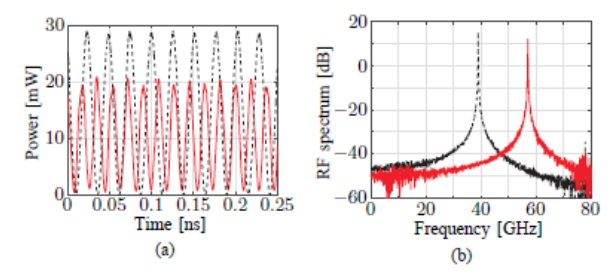


Fig. 7: Two examples of self-pulsation results obtained for $I_S=I_M=30\,\mathrm{mA}$ for two different values of ϕ_S : in (a) the time domain signals and in (b) the corresponding RF spectrum. Dashed black line results for the minimum value of $f_{\mathrm{PPR}}\approx40\,\mathrm{GHz}$ and continuous red line results for $f_{\mathrm{PPR}}\approx57\,\mathrm{GHz}$.

The dashed curve in Fig. 6c represents an operation condition whose response is practically equal to that of a corresponding single section DBR laser; the effect of the coupled cavity DBR configuration can be directly obtained comparing the other results with this one. Furthermore we put in evidence that the borders between the various regions are "soft" in the sense that one should consider a gradual transition of the laser behavior from region (B), (C) and (D). A more sharp transition has been typically found at the border with region (A-SP).

We discuss now for brevity only the results obtained for one of the 6 structures indicated with markers in Fig. 4 and analyzed with the dynamic simulation: the laser cavity indicated with a squared marker in Fig. 4b, with $\kappa=100\,\mathrm{cm^{-1}},$ $L_{gr,L}=181\,\mathrm{\mu m},$ $L_{M}=L_{S}=250\,\mathrm{\mu m},$ $L_{gc,C}=82\,\mathrm{\mu m},$ right facet as cleaved, and having a threshold current density $J_{th}=24\,\mathrm{mA\,mm^{-1}}.$ For this laser operating in the region

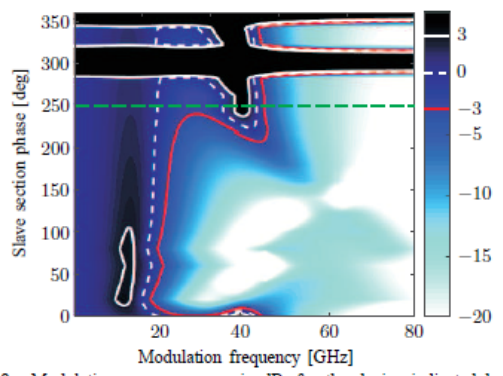


Fig. 8: Modulation response map, in dB, for the device indicated by the red square marker in Fig. 4b, with in the ordinate the phase shift phi_M introduced in the Slave optical cavity. The output power is approximately $25\,\mathrm{mW}$; $I_S=60\,\mathrm{mA}$, $I_M=8\,\mathrm{mA}$. Contour lines indicate $-3\,\mathrm{dB}$ (red line), $0\,\mathrm{dB}$ (white dashed line), and $3\,\mathrm{dB}$ (white continuous line) levels of the modulation response. The green dashed horizontal line indicates the operation condition chosen for the large signal operation.

(D) of Fig. 6a, we report in detail the results obtained only for one of the bias points allowing high speed large signal modulation. The small signal modulation results are show in Fig. 8 color map where in the abscissa is reported the modulation frequency and in the ordinates the static phase change in the Slave section to tune the position of the cavity modes to obtain an operation condition allowing the extension of the modulation bandwidth.

The two dark horizontal strips represent regions of selfpulsation similar to those in region (A-SP) in Fig. 6a. The blue "horn" pointing to the lower part of the map represents the PPR variation in the modulation characteristic that when is at high frequency is attenuated and become stronger as the mode separation decreases. In the lower part of the map this effect does not appear because in this range of phases the closest side mode is on the shorter wavelength side respect to the lasing mode and in this condition the PPR effect do not take place [12]. For the value of Slave cavity phase highlighter by the dashed horizontal line, the value of the PPR frequency is around $40\,\mathrm{GHz}$, in good agreement with the f_{PPR} value used to choose the cavity parameters from the map in Fig. 4;

TABLE I: Main material parameters used for the FDTW simulations.

Symbol	Description	Value
n_{eff}	Effective refractive index	3.2
n_q	Group refractive index	3.6
Γ_{xy}	Transversal optical	17%
	confinement factor	
N_0	Carrier density at transparency	$1 \times 10^{18} \mathrm{cm}^{-3}$
a_0	Active region differential gain	$13 \times 10^{-16} \mathrm{cm}^2$
$\alpha_{i,A}$	Active region intrinsic losses	$10{\rm cm}^{-1}$
$\alpha_{i,G}$	Grating region intrinsic losses	$10{\rm cm}^{-1}$
λ_B	Bragg wavelength	1.550 µm
α_{LEF}	Linewidth enhancement factor	3
ε	Non linear gain compression factor	$5 \times 10^{-17} \text{cm}^3$
A	Mono-molecular	$1.4\mathrm{ns^{-1}}$
	recombination coefficient	
B	Bi-molecular	$0.1{\rm cm^3ns^{-1}}$
	recombination coefficient	
C	Auger recombination coefficient	$7.5 \mathrm{cm}^6 \mathrm{ns}^{-1}$

this result confirms the reliability of the proposed design procedure.

We investigated also how the small signal dynamic characteristics are affected by the change of some of the material parameters as the gain saturation ε and the linewidth enhancement factor α_{LEF} . We varied in a wide range the gain saturation from $\varepsilon = 2 \times 10^{-17} \, \mathrm{cm}^3$ to $\varepsilon = 8 \times 10^{-17} \, \mathrm{cm}^3$ and the results for the two extreme values are reported in Fig. 10 where the position of the PPR peak is found practically unchanged; a moderate variation of the self-pulsation region and a significant reduction of the CPR peak when increasing the gain saturation can be observed. More significant are the effects of the linewidth enhancement factor which was varied from $\alpha_{LEF} = 1$ to $\alpha_{LEF} = 5$. In Fig. 9 we reported the cases of $\alpha_{LEF}=2$ and $\alpha_{LEF}=4$. The area of self-pulsation increases increasing α_{LEF} ; while this increase is moderate for $\alpha_{LEF} = 4$ it becomes significant for $\alpha_{LEF} = 5$. An opposite behavior is obtained decreasing this parameter: for $\alpha_{LEF} = 1$ the region of self-pulsation disappears while the region showing the PPR effect is confined in a reduced range of the Slave cavity phases variation range.

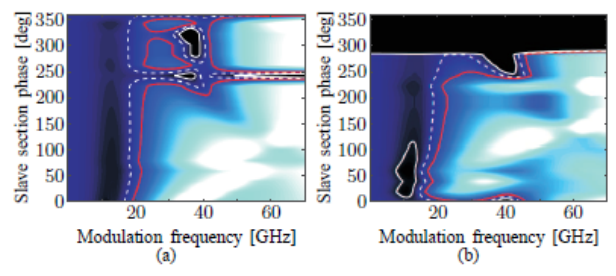


Fig. 9: Modulation response maps, in dB, for the case in Fig. 8 with $\alpha LEF = 2$ and 4 in (a) and (b), respectively. Same notations as in Fig. 8.

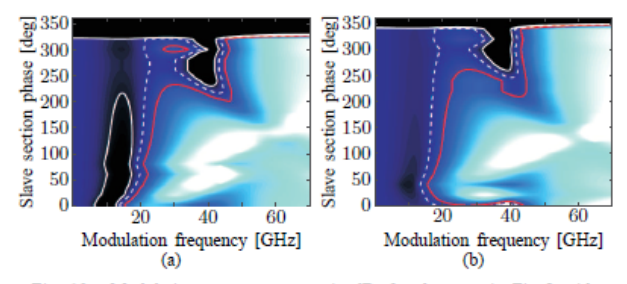


Fig. 10: Modulation response maps, in dB, for the case in Fig. 8 with ε =2 \times $10^{-17}\,\rm cm^3$ and $8\times10^{-17}\,\rm cm^3$ in (a) and (b), respectively. Same notations as in Fig. 8.

The same device considered in Fig. 8 was tested using the FDTW code for the large signal modulation. For this analysis, the Master section current was kept constant, and a non-return-to-zero (NRZ) Pseudo Random Bit Sequence (PRBS) composed by $2^{15}-1$ bits was applied to the Slave section. The Slave section phase ϕ_S was set to 250° (dashed horizontal line in Fig. 8) in order to take advantage of the bandwidth extension provided by the PPR effect.

Results are presented as eye diagrams in Fig. 11. For each eye, on the right axes we report the output power P, while on

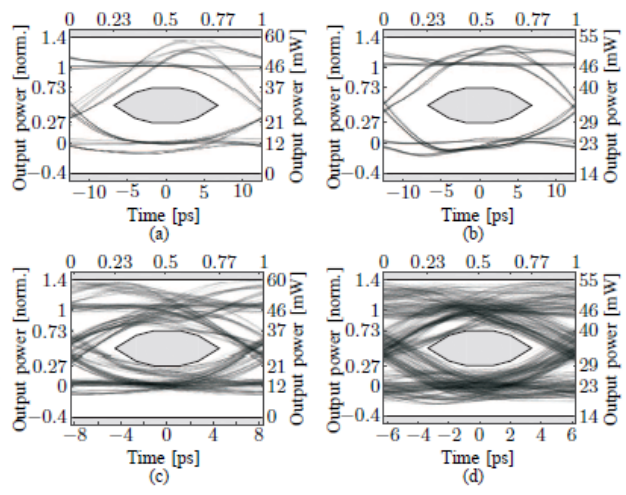


Fig. 11: . Eye diagrams for the device considered in Fig. 6 using $\phi_S=250^\circ$, computed with a $2^{15}-1$ bits long NRZ PRBS sequence. $I_M=8$ mA. (a) $I_{S,0}=40$ mA, $I_{S,1}=110$ mA, corresponding to a 6 dB modulation amplitude, with a 40 Gbit/s repetition frequency, increases to 60 Gbit/s in (c). (b) $I_{S,0}=60$ mA, $I_{S,1}=110$ mA, corresponding to a 3 dB modulation amplitude, with a 40 Gbit/s repetition frequency, increased to 80 Gbit/s in (d).

the left vertical axes we indicate P normalized with respect to the bit "0" and "1" levels P_0 and P_1 : $p = (P-P_0)/(P_1-P_0)$. In order to allow for an easy estimation of the eyes opening, in the Figure we also report the limits for optical transmission systems indicated by the IEEE P802.3ba standard [32].

As expected, the results reported in Fig. 11a,b show that open eyes can be obtained using a $40\,\mathrm{Gbit/s}$ repetition rate when $P_1/P_0=6\,\mathrm{dB}$ (a) and $P_1/P_0=3\,\mathrm{dB}$ (b).

We then increased the repetition rate and found that the upper limit allowed to obtain an open eye diagram is $60\,\mathrm{Gbit/s}$ when operating with $P_1/P_0=6\,\mathrm{dB}$ (c) and $80\,\mathrm{Gbit/s}$ when $P_1/P_0=3\,\mathrm{dB}$ (d), which indicates an extension of the modulation frequency well above the CPR and PPR frequencies. The eyes are finally closed when higher bit rates are used.

IV. CONCLUSION

We proposed a design procedure to exploit the PPR effect in an integrated device composed by two mutually coupled DBR lasers. The design maps, obtained using the transmission matrix method, allow for a proper choice of the cavity parameters once the required bandwidth extension and the technological aspects have been defined.

The proposed designs have been numerically validated using a FDTW code. With a proper tuning of the cavity modes position, the composite laser small signal modulation response shows an increase of the $-3 \, \mathrm{dB}$ modulation bandwidth thanks to the PPR peak appearing close to the design frequency, thus endorsing the design guidelines. The dependence of the PPR on material parameters such as the linewidth enhancement factor and the gain compression factor has been discussed. Finally, the large signal modulations with PRBS signals allowed to obtain eye diagrams which are open up to $60 \, \mathrm{Gbit/s}$ and $80 \, \mathrm{Gbit/s}$ with an amplitude of $6 \, \mathrm{dB}$ and $3 \, \mathrm{dB}$, respectively.

Acknowledgement

Sandia National Laboratories is a multi-program laboratory managed and operated by Sandia Corporation, a wholly owned subsidiary of Lockheed Martin Corporation, for the U. S. Department of Energy's National Nuclear Security Administration under contract DE-AC04-94AL85000.

REFERENCES

- [1] G. de Valicourt, G. Levaufre, Y. Pointurier, A. Le Liepvre, J.-C. Antona, C. Jany, A. Accard, F. Lelarge, D. Make, and G.-H. Duan, "Direct Modulation of Hybrid Integrated InP/Si Transmitters for short and long reach access network," *Lightwave Technology, Journal of*, vol. PP, no. 99, 2015
- [2] L. A. Coldren, S. W. Corzine, and M. L. Maănović, Diode Lasers and Photonic Integrated Circuits. New York: Wiley, 2012.
- [3] I. Montrosset and P. Bardella, "Laser dynamics providing enhancedmodulation bandwidth," in SPIE Photonics Europe. International Society for Optics and Photonics, 2014.
- [4] K. Vahala and A. Yariv, "Detuned loading in coupled cavity semiconductor lasers-effect on quantum noise and dynamics," Applied Physics Letters, vol. 45, no. 5, pp. 501-503, 1984. [Online]. Available: http://scitation.aip.org/content/aip/journal/apl/45/5/10.1063/1.95316
- [5] K. Vahala, J. Paslaski, and A. Yariv, "Observation of modulation speed enhancement, frequency modulation suppression, and phase noise reduction by detuned loading in a coupled—cavity semiconductor laser," Applied Physics Letters, vol. 46, no. 11, pp. 1025–1027, 1985. [Online]. Available: http://scitation.aip.org/content/aip/journal/apl/46/11/10.1063/1.95799
- [6] U. Feiste, "Optimization of modulation bandwidth in DBR lasers with detuned Bragg reflectors," Quantum Electronics, IEEE Journal of, vol. 34, no. 12, pp. 2371–2379, Dec 1998.
- [7] O. Kjebon, R. Schatz, S. Lourdudoss, S. Nilsson, B. StAlnacke, and L. Backbom, "Two-section InGaAsP DBR-lasers at 1.55

 µm wavelength with 31 GHz direct modulation bandwidth," in *Indium Phosphide* and Related Materials, International Conference on, May 1997, pp. 665– 688
- [8] M. Chaciński and R. Schatz, "Impact of losses in the Bragg section on the dynamics of detuned loaded DBR lasers," *Quantum Electronics*, *IEEE Journal of*, vol. 46, no. 9, pp. 1360–1367, Sept 2010.
- [9] X. Pan, H. Olesen, and B. Tromborg, "Modulation characteristics of tunable DFB/DBR lasers with one or two passive tuning sections," *Quantum Electronics, IEEE Journal of*, vol. 25, no. 6, pp. 1254–1260, Jun 1989
- [10] O. Kjebon, R. Schatz, S. Lourdudoss, S. Nilsson, B. StAlnacke, and L. Backbom, "30 GHz direct modulation bandwidth in detuned loaded InGaAsP DBR lasers at 1.55 μm wavelength," *Electronics Letters*, vol. 33, no. 6, pp. 488–489, Mar 1997.
- [11] L. Bach, W. Kaiser, J. P. Reithmaier, A. Forchel, T. Berg, and B. Tromborg, "Enhanced direct-modulated bandwidth of 37 GHz by a multi-section laser with a coupled-cavity-injection-grating design," *Electronics Letters*, vol. 39, no. 22, pp. 1592-1593, Oct 2003.
- [12] P. Bardella and I. Montrosset, "A New Design Procedure for DBR Lasers Exploiting the Photon-Photon Resonance to Achieve Extended Modulation Bandwidth," Selected Topics in Quantum Electronics, IEEE Journal of, vol. 19, no. 4, pp. 1502 408-1502 408, July 2013.
- [13] J. P. Reithmaier, W. Kaiser, L. Bach, A. Forchel, V. Feies, M. Gioannini, I. Montrosset, T. Berg, and B. Tromborg, "Modulation speed enhancement by coupling to higher order resonances: a road towards 40 ghz bandwidth lasers on inp," in *Indium Phosphide and Related Materials*, 2005. International Conference on, May 2005, pp. 118-123.
- [14] J. Reithmaier, L. Bach, and W. Kaiser, "Multisectional laser," Aug. 4 2009, US Patent 7,570,681. [Online]. Available: http://www.google.com/patents/US7570681

- [19] F. Grillot, C. Wang, N. Naderi, and J. Even, "Modulation properties of self-injected Quantum-Dot semiconductor diode lasers," *Selected Topics in Quantum Electronics, IEEE Journal of*, vol. 19, no. 4, pp. 1900 812– 1900 812, July 2013.
- [20] T. B. Simpson, J. Liu, and A. Gavrielides, "Bandwidth enhancement and broadband noise reduction in injection-locked semiconductor lasers," *Photonics Technology Letters, IEEE*, vol. 7, no. 7, pp. 709-711, July 1995.
- [21] A. Murakami, K. Kawashima, and K. Atsuki, "Cavity resonance shift and bandwidth enhancement in semiconductor lasers with strong light injection," *Quantum Electronics, IEEE Journal of*, vol. 39, no. 10, pp. 1196–1204, Oct 2003.
- [22] E. Lau, L. J. Wong, and M. Wu, "Enhanced modulation characteristics of optical injection-locked lasers: A tutorial," *Selected Topics in Quantum Electronics, IEEE Journal of*, vol. 15, no. 3, pp. 618–633, May 2009.
- [23] A. Enard, P. Resneau, M. Calligaro, O. Parillaud, M. Krakowski, M. Vallone, P. Bardella, and I. Montrosset, "Mode locking and bandwidth enhancement in single section ridge laser with two spatial modes." in Semiconductor Laser Conference (ISLC), 2010 22nd IEEE International, Sept 2010, pp. 113–114.
- Sept 2010, pp. 113-114.

 [24] H. Dalir and F. Koyama, "High-speed operation of bow-tie-shaped oxide aperture VCSELs with photon-photon resonance," Applied Physics Express, vol. 7, no. 2, p. 022102, 2014.
- [25] —, "Highly stable operations of transverse-coupled cavity VCSELs with enhanced modulation bandwidth," *Electronics Letters*, vol. 50, no. 11, pp. 823–824, 2014.
- [26] F. Gerschütz, M. Fischer, J. Koeth, I. Krestnikov, A. Kovsh, C. Schilling, W. Kaiser, S. Höfling, and A. Forchel, "1.3 μm Quantum Dot laser in coupled-cavity-injection-grating design with bandwidth of 20 GHz under direct modulation," Opt. Express, vol. 16, no. 8, pp. 5596–5601, Apr 2008. [Online]. Available: http://www.opticsexpress.org/abstract.cfm?URI=oe-16-8-5596
- [27] W. Chow, Z. Yang, G. Vawter, and E. Skogen, "Modulation response improvement with isolator-free injection-locking," *IEEE Photonics Tech*nology Letters, vol. 21, no. 13, p. 839, 2009.
- [28] Z. Yang, A. Tauke-Pedretti, G. Vawter, and W. Chow, "Mechanism for Modulation Response Improvement in Mutually Injection-Locked Semiconductor Lasers," *Quantum Electronics, IEEE Journal of*, vol. 47, no. 3, pp. 300–305, March 2011.
- [29] A. Tauke-Pedretti, G. Vawter, E. Skogen, G. Peake, M. Overberg, C. Alford, W. Chow, Z. Yang, D. Torres, and F. Cajas, "Mutual Injection Locking of Monolithically Integrated Coupled-Cavity DBR Lasers," *Photonics Technology Letters, IEEE*, vol. 23, no. 13, pp. 908–910, July 2011.
- [30] A. Tauke-Pedretti, E. Skogen, G. Vawter, and W. Chow, "Mutually injection locked lasers for enhanced frequency response," Apr. 1 2014, US Patent 8,687,665. [Online]. Available: https://www.google.com/patents/US8687665
- [31] P. Bardella and I. Montrosset, "Analysis of self-pulsating three-section DBR lasers," Selected Topics in Quantum Electronics, IEEE Journal of, vol. 11, no. 2, pp. 361-366, March 2005.
 [32] IEEE 802.3-2008 IEEE Standard for Information Technology-
- [32] IEEE 802.3-2008 IEEE Standard for Information Technology-Specific Requirements-Part 3: Carrier Sense Multiple Access with Collision Detection (CMSA/CD) Access Method and Physical Layer Specifications [Online]. [Online]. Available: http://standards.ieee.org/getieee802/ download/802.3ba-2010.pdf

- [14] J. Reithmaier, L. Bach, and W. Kaiser, "Multisectional laser," Aug. 4 2009, US Patent 7,570,681. [Online]. Available: http://www.google.com/patents/US7570681
- nmp://www.googie.com/patents/US/3/0681

 [15] F. Gerschütz, M. Fischer, J. Koeth, I. Krestnikov, A. Kovsh, C. Schilling, W. Kaiser, S. Höfling, and A. Forchel, "1.3 \(\mu\)m Quantum Dot laser in coupled-cavity-injection-grating design with bandwidth of 20 GHz under direct modulation," Opt. Express, vol. 16, no. 8, pp. 5596–5601, Apr 2008. [Online]. Available: http://www.opticsexpress.org/abstract.cfm?URI=oe-16-8-5596
- [16] M. Vallone, P. Bardella, and I. Montrosset, "Enhanced Modulation Bandwidth in Complex Cavity Injection Grating Lasers," *Quantum Electronics, IEEE Journal of*, vol. 47, no. 10, pp. 1269–1276, Oct 2011.
- [17] M. Radziunas, A. Glitzky, U. Bandelow, M. Wolfrum, U. Troppenz, J. Kreissl, and W. Rehbein, "Improving the Modulation Bandwidth in Semiconductor Lasers by Passive Feedback," Selected Topics in Quantum Electronics, IEEE Journal of, vol. 13, no. 1, pp. 136–142, Jan 2007.
- [18] G. Morthier, R. Schatz, and O. Kjebon, "Extended modulation band-width of DBR and external cavity lasers by utilizing a cavity resonance for equalization," *Quantum Electronics, IEEE Journal of*, vol. 36, no. 12, pp. 1468–1475, Dec 2000.